CHEMISTRY
A EUROPEAN JOURNAL

DOI: 10.1002/chem.201203290

Luminescent Platinum(II) Complexes of 1,3-Bis(*N*-alkylbenzimidazol-2′-yl)benzene-Type Ligands with Potential Applications in Efficient Organic Light-Emitting Diodes

Elizabeth Suk-Hang Lam, Daniel Ping-Kuen Tsang, Wai Han Lam, Anthony Yiu-Yan Tam, Mei-Yee Chan,* Wing-Tak Wong, and Vivian Wing-Wah Yam*[a]

Abstract: A series of luminescent platinum(II) complexes of tridentate 1,3-bis(*N*-alkylbenzimidazol-2′-yl)benzene (bzimb) ligands has been synthesized and characterized. One of these platinum(II) complexes has been structurally characterized by X-ray crystallography. Their electrochemical, electronic absorption, and luminescence properties have been investigated. Computational studies have been performed on this class of complexes to elucidate the origin of their photophysical properties. Some of these complexes have been utilized in the fabrication of organic light-emitting diodes (OLEDs) by using either vapor deposition or spin-coating techniques. Chloroplatinum(II)–bzimb complexes that are functionalized at the 5-position of the aryl ring, [Pt(R-bzimb)Cl], not only show tunable emission color but also exhibit high current and external quantum efficiencies in OLEDs. Concentration-dependent dual-emissive behavior was observed in multilayer OLEDs upon the incorporation of pyrenyl ligand into the Pt(bzimb) system. Devices doped with low concentrations of the complexes gave rise to white-light emission, thereby representing a unique class of small-molecule, platinum(II)-based white OLEDs.

Keywords: density functional calculations · cyclometalation · luminescence · organic light-emitting diodes · platinum

Introduction

Organic light-emitting diodes (OLEDs) have recently become popular candidates for research into lighting technology, owing to their potential applications in solid-state lighting and flat-panel displays, because they offer the distinct advantages of high luminous efficiency, a full-color gamut, and low manufacturing costs.[1] In particular, phosphorescent organic light-emitting diodes (PHOLEDs) are of growing interest because of their ability to harvest both singlet and triplet excitons for light emission through electron–hole recombination upon electrical excitation,[2–4] thereby increasing their internal quantum efficiency, which can theoretically reach unity at room temperature.[3] Platinum, as a heavy atom and with strong spin-orbit coupling that can facilitate intersystem crossing for harvesting all singlet and triplet excitons, has attracted much attention over the past few decades.

Among various metal complexes, cyclometalated platinum(II) systems display strong phosphorescence and electroluminescence (EL) and they could be utilized as light-emitting materials in OLEDs.[4] One typical example is the class of platinum(II) systems with the incorporation of a C^N^N ligand, 6-phenyl-2,2′-bipyridine, which has been demonstrated to be useful for the fabrication of highly efficient OLEDs with a maximum luminance of 63 000 cd m^{-2}.[4b] Another class of platinum(II) N^C^N complexes of 1,3-dipyridylbenzene has also been reported to exhibit strong phosphorescence with excellent PHOLED performance.[4d–f] It has been shown that the emission color and energy of these devices can be readily tuned by incorporating different functional groups onto the phenyl moiety.[4d,e]

Despite the use of 6-phenyl-2,2′-bipyridine and 1,3-dipyridylbenzene as cyclometalating ligands, another new class of cyclometalating ligands, namely 1,3-bis(*N*-alkylbenzimidazol-2′-yl)benzene (bzimb) ligands, has been used over the past decade.[4a,g,5] This type of cyclometalating ligands has previously been studied in iridium(III)[5a] and palladium(II)[5b] systems. On the other hand, there have been no reports on the synthesis and spectroscopic properties of platinum(II) complexes of this ligand until very recently, when we reported its coordination to the platinum(II) system.[4a] This new class of luminescent platinum(II) complexes exhibits bright-green EL and good PHOLED performance, with a high current efficiency of 38.9 cd A^{-1} and an external quantum efficiency (EQE) of 11.5 %.[4a]

---

[a] E. S.-H. Lam, D. P.-K. Tsang, Dr. W. H. Lam, Dr. A. Y.-Y. Tam,
Dr. M.-Y. Chan, Prof. Dr. W.-T. Wong, Prof. Dr. V. W.-W. Yam
Department of Chemistry, The University of Hong Kong
Pokfulam Road (Hong Kong)
Fax: (+852) 2857-1586
E-mail: chanmym@hku.hk
wwyam@hku.hk

Supporting information for this article is available on the WWW under http://dx.doi.org/10.1002/chem.201203290.

Although these platinum(II) complexes of the bzimb ligand have interesting photophysical properties, there is still room for improvement and optimization to develop high-efficiency OLEDs. Challenges relating to color stability and tunability, as well as the selection of suitable metal complexes for high-efficiency PHOLEDs with low manufacturing costs, are yet to be overcome.

Herein, we report the synthesis, characterization, and electrochemical and photophysical properties of a class of luminescent Pt(bzimb) complexes. PHOLEDs of these complexes were prepared by either thermal evaporation or spin-coating techniques. With the aim of tuning emission energies without sacrificing the performance of devices based on the [Pt(bzimb)Cl] system, we functionalized the bzimb ligand at the 5-position of the phenyl ring and successfully fine-tuned the emission energy and fabricated PHOLEDs with high current efficiencies and EQEs. Interestingly, upon incorporation of a pyrenylalkynyl ligand, one of the mononuclear organometallic complexes was found to exhibit dual emission in the red and green regions, the color of which could be varied by controlling the concentration of the dopant. Apart from the utilization of blue, green, and red molecular emitters in multiple layers,[1a,6] or the combination of simultaneous monomer and excimer EL[7] to generate white light, there are only a limited number of complexes of iridium(III) that can emit white light from a single molecule.[8] This work should provide an interesting insight into the future design and development of white OLEDs (WOLEDs). In addition, two devices that exhibit green emission with high efficiencies have been fabricated by using alkynylcarbazole-containing Pt(bzimb) complexes. Density functional theory (DFT) and time-dependent density functional theory (TDDFT) calculations have also been performed on this class of complexes to gain a deeper understanding of their photophysical properties.

Results and Discussion

Synthesis and characterization: Complexes **2** and **3** were synthesized according to a modified procedure for the synthesis of complex **1**, which was reported recently.[4a] The reaction mixture was heated under reflux in glacial acetic acid for 3 days (Figure 1). Complexes **4**, **5**, **7**, and **8** were synthesized by the reaction of complex **1** with the corresponding alkynes in the presence of sodium hydroxide in CH_2Cl_2 and MeOH under refluxing conditions, similar to that reported for complex **6**,[4g] to give the desired complexes (Scheme 1). The identities of all of the newly synthesized platinum(II)–bzimb complexes were confirmed by ^{1}H NMR spectroscopy, MS (FAB), and elemental analysis. Complex **7** was also structurally characterized by X-ray crystallography.

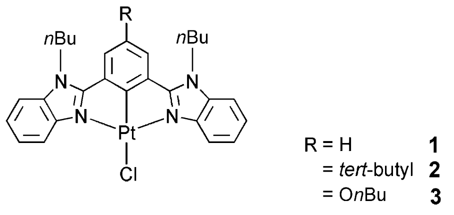

Figure 1. Molecular structures of chloroplatinum(II)–bzimb complexes **1**–**3**.

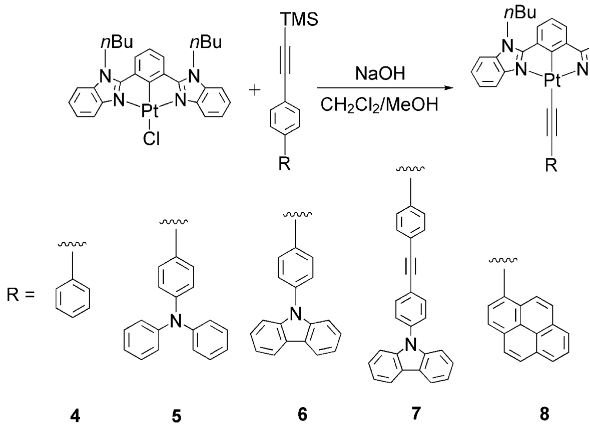

Scheme 1. Synthetic route to and molecular structures of complexes **4**–**8**.

X-ray crystallography: Similar to complex **1**,[4a] complex **7** adopts a distorted square-planar geometry, owing to the steric demands of the bzimb ligand, as shown by the C15–Pt1–N1 and C15–Pt1–N2 angles (78.6–79.9°) and the N1–Pt1–N2 angle (158.4°). The Pt–C(alkynyl) bond length (2.031 Å) in complex **7** is longer than that in the related platinum(II)–bzimpy system.[9] This difference has been attributed to a stronger *trans* influence exerted by the anionic phenyl ring on the bzimb ligand compared to the pyridyl unit on the bzimpy ligand. The Pt–N and Pt–C(bzimb) bond lengths are 2.006–2.027 Å and 1.955 Å, respectively. The Pt–C(bzimb) bond length in complex **7** is longer than that in complex **1** (1.931 Å),[4a] which is due to a stronger *trans* influence of the alkynyl ligand than that of the chloro ligand. The crystal data are summarized in the Supporting Information, Table S1. The structure and crystal packing of complex **7** are shown in Figure 2 and the Supporting Information, Figure S1, respectively. The interplanar angle between the two alkynyl aryl rings is 15.1° and that between the carbazole unit and the adjacent aryl ring is 79.8°. The intermolecular Pt···Pt distance between two adjacent molecules is 5.18 Å, which indicates the absence of Pt···Pt interactions. The interplanar distance between the bzimb planes of two adjacent molecules is 3.46 Å, which may indicate the presence of weak π–π interactions between the two bzimb planes.

Electrochemistry: Cyclic voltammetry was performed for these complexes in CH_2Cl_2 with 0.1 M nBu$_4$NPF$_6$ as a supporting electrolyte. The electrochemical data are summarized in Table 1 and a cyclic voltammogram of complex **5** in CH_2Cl_2 (with 0.1 M nBu$_4$NPF$_6$) is shown in the Supporting

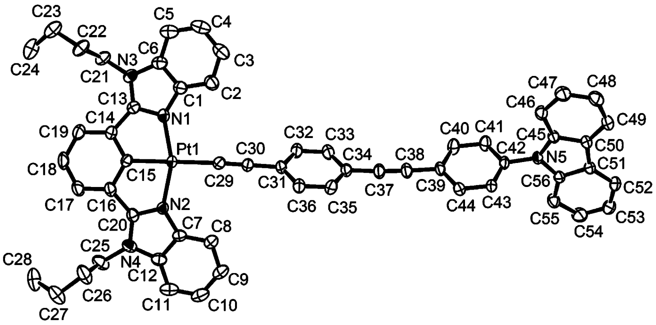

Figure 2. Perspective drawing of complex **7** with atom numbering; hydrogen atoms are omitted for clarity. Thermal ellipsoids are set at 30% probability.

Table 1. Electrochemical data for complexes **1**–**8**.

Complex	Oxidation $E_{1/2}$ (E_{pa}) [V] versus SCE[a,b]	Reduction E_{pc} [V] versus SCE[c]
1	(+1.00), (+1.44), (+1.79)	−1.97
2	(+0.99), (+1.46), (+1.79)	−1.97
3	(+0.91), (+1.43), (+1.88)	−1.85
4	(+0.79), (+1.85)	−2.05
5	(+0.60), +1.00, (+1.79)	−2.08
6[d]	(+0.75), +1.37, (+1.78)	−1.99
7	(+0.74), +1.37, (+1.79)	−1.99
8	(+0.64), (+1.77)	−2.00

[a] $E_{1/2}$ refers to the quasi-reversible anodic peak, calculated according to the equation $E_{1/2}=(E_{pa}+E_{pc})/2$, in which E_{pa} and E_{pc} are the peak anodic and cathodic potentials, respectively. [b] Values in parentheses refer to the anodic peak potential (E_{pa}) for the irreversible oxidation waves. [c] E_{pc} refers to the cathodic peak potential for the irreversible reduction waves. [d] Taken from ref. [4g].

Information, Figure S2. An irreversible reduction wave for complexes **1**–**8** was observed between −1.85 and −2.08 V versus the standard calomel electrode (SCE). This irreversible reduction wave was found to be insensitive towards the nature of the alkynyl ligands. This result could possibly be due to a bzimb-based reduction, as supported by the DFT calculations (see below). Slight variation with the substituents on the bzimb ligand was observed, which may be due to the inductive effect of the substituents at the 5-position of the aryl ring (see below). In complexes **1**–**3**, three irreversible oxidation waves were observed, whereas, in complexes **4**–**8**, an irreversible wave was observed within the range +0.60 to +0.79 V (versus SCE). The potential for the oxidation wave was found to vary with the electronic effects of the alkynyl ligands. For example, complex **5**, which possesses the more electron-rich triphenylaminoalkynyl ligand, has a less-positive potential (+0.60V versus SCE) than that of complex **4**, which possesses a phenylalkynyl ligand (+0.79V versus SCE). This suggests that the oxidation was alkynyl-ligand based with mixing of a metal-centered contribution. This assignment was further supported by the observation that complex **8**, with a more π-conjugated pyrenylalkynyl ligand, was more readily oxidized than complex **4**, because its extended π-conjugation would render the π(C≡C−R)/dπ(Pt) orbital higher-lying in energy. The irreversible oxidative wave at about +1.77 V versus SCE was found to be rather insensitive to the nature of the alkynyl ligands that were employed, possibly resulting from an irreversible $Pt^{II}\rightarrow Pt^{III}$ oxidation. A quasi-reversible oxidation couple was observed in complexes **5**–**7**. The wave at +1.00 V versus SCE in complex **5** is probably attributed to the oxidation of the triphenylamine unit,[10] whereas the wave at about +1.37 V in complexes **6** and **7** is tentatively assigned to the oxidation of carbazole.[4g,11]

Electronic absorption spectroscopy: Complexes **1**–**3** show a higher-energy band at about 306 nm and a lower-energy band at around 352–432 nm, as shown in Figure 3. The photophysical data of complexes **1**–**8** are summarized in Table 2. A significant red-shift is observed in the lower-energy band on going from complex **1** to complex **3**, probably because the electron-donating substituent on the benzene unit of bzimb destabilizes the HOMO energy level, thereby leading to a narrowing of HOMO–LUMO energy gap (see below).

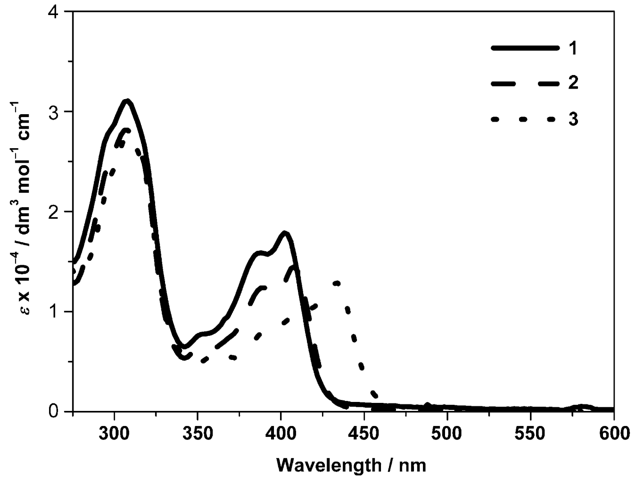

Figure 3. Electronic absorption spectra of complexes **1**–**3** in CH_2Cl_2 at room temperature.

The electronic absorption spectra of most of the alkynyl complexes show a higher-energy absorption band at around 284–345 nm and a lower-energy absorption band at around 360–409 nm (see the Supporting Information, Figure S3). The higher-energy absorptions are assigned to intraligand (IL) π→π* transitions (bzimb and alkynyl units), whereas the lower-energy absorptions are ascribed to IL π→π* transitions in the bzimb ligand, with substantial mixing of metal-to-ligand charge transfer (MLCT) [dπ(Pt)→π*(bzimb)] and ligand-to-ligand charge transfer (LLCT) [π(C≡C-R)→π*-(bzimb)] character.[4g,9] For complexes **7** and **8**, the absorption band in the lower-energy region has a larger molar extinction coefficient than that of complex **4**. It is possible that the absorption band in complexes **7** and **8** would also consist of a metal-perturbed IL π→π* transition of the alkynyl ligand. This result is further supported by the TDDFT calculations (see below).

Table 2. Photophysical data for complexes **1**–**8**.

Complex	Medium (T [K])	Electronic absorption λ_{max} [nm] (ε [dm^{3}mol^{-1}cm^{-1}])	Emission λ_{em} [nm] (τ_0 [μs])	Φ_{PL} in solution
1	CH_2Cl_2[a] (298)	306 (30960), 352 (7730), 384 (15820), 402 (17865)	506, 544, 587 (5.3)	0.19[e]
	solid[b] (298)		520, 546, 593 (0.5)	
	solid[b] (298)		520, 543, 564 (5.5)	
	glass[c] (77)		491, 530, 574 (7.9)	
	thin film[d] (298)		513, 551, 603	0.78
2	CH_2Cl_2[a] (298)	306 (27880), 352 (6770), 388 (12340), 407 (14665)	507, 547, 595 (6.4)	0.25
	solid[b] (298)		509, 544, 592, 641 (1.5)	
	solid[b] (77)		525, 568, 621 (5.5)	
	glass[c] (77)		495, 534, 579, 637 (9.6)	
	thin film[d] (298)		514, 552, 602	0.70
3	CH_2Cl_2[a] (298)	306 (27360), 362 (5760), 388 (7865), 408 (9710), 432 (12780)	530, 572, 624 (5.8)	0.15
	solid[b] (298)		526, 565, 617 (1.2)	
	solid[b] (77)		538, 580, 634 (8.8)	
	glass[c] (77)		518, 560, 610 (12.8)	
	thin film[d] (298)		535, 580, 628	0.55
4	CH_2Cl_2[a] (298)	284 (35540), 310 (32115), 364 (14030), 390 (13070), 409 (12050)	509, 548, 593	0.22
	solid[b] (298)		505, 541, 590 (2.2)	
	solid[b] (77)		519, 563, 613 (3.8)	
	glass[c] (77)		492, 532, 576, 630 (8.2)	
	thin film[d] (298)		514, 551, 602	0.77
5	CH_2Cl_2[a] (298)	300 (34745), 312 (38285), 380 (17660), 403 (13290)	510, 547, 595	0.67
	solid[b] (298)		510, 550, 615 (3.2)	
	solid[b] (77)		434, 521, 564, 614, 730 (2.5)	
	glass[c] (77)		493, 533, 577, 625 (6.9)	
	thin film[d] (298)		514, 552, 603	0.71
6	CH_2Cl_2[a,f] (298)	292 (90770), 306 (78330), 345 (25120), 366 (26690), 385 (23610), 408 (18005)	509, 548, 595	0.51
	solid[b,f] (298)		505, 540, 584 (1.7)	
	solid[b,f] (77)		500, 540, 625 (7.6)	
	glass[c,f] (77)		490, 531, 575 (8.1)	
	thin film[d] (298)		514, 551, 600	0.78
7	CH_2Cl_2[a] (298)	294 (46755), 316 (52340), 338 (49840), 370 (42605), 404 (17260)	507, 535, 595	0.46
	solid[b] (298)		468, 512, 538, 664 (1.2)	
	solid[b] (77)		531, 567, 594, 651 (5.3)	
	glass[c] (77)		493, 525, 557, 573, 593, 629 (8.4)	
	thin film[d] (298)		514, 543, 600	0.52
8	CH_2Cl_2[a] (298)	293 (63045), 360 (35330), 384 (26370), 402 (26775)	507, 547, 593, 659, 719, 737	0.09
	solid[b] (298)		467, 497, 645 (4.7)	
	solid[b] (77)		467, 497, 645 (5.3)	
	glass[c] (77)		490, 526, 564 (8.8) 650, 669, 707, 725, 752, 776 (0.8)	
	thin film[d] (298)		661, 736	0.02

[a] Measured at a concentration of 1×10^{-5} M. [b] Solid-state emission was recorded after grinding. [c] In butyronitrile glass. [d] 5 wt.% in MCP. [e] Taken from ref. [4a]. [f] Taken from ref. [4g].

Luminescence spectroscopy: All of these complexes, except complex **8**, exhibit strong green luminescence in solution, 77 K glass, and in the solid state. The large Stokes shifts suggest that the emissions are of triplet parentage. The photoluminescence quantum yields (Φ_{PL}) of chloro complexes **1**–**3** range from 0.15 to 0.25, whilst alkynyl complexes **4**–**7** have higher Φ_{PL} (0.22–0.67). All of the complexes give higher Φ_{PL} than their bzimpy counterparts (bzimpy = 2,6-bis(*N*-alkylbenzimidazol-2′-yl)pyridine).[9] This result may be attributed to the presence of an anionic phenyl ring on the bzimb ligand, which substantially raises the energy of the d–d excited state, thereby decreasing the rate of nonradiative deactivation pathways. In CH_2Cl_2, complexes **1**–**6** exhibit a vibronic-structured emission at around 507–530 nm, with vibrational progressional spacings of about 1380 cm^{-1}. The vibrational progressional spacings correspond to typical aromatic vibrational modes of the bzimb ligand. The emission probably originated from the triplet IL excited state of the cyclometalated ligand,[4a] which is further supported by its sensitivity towards the substituent at the 5-position of the bzimb ligand, as demonstrated by complexes **1**–**3**. Although the emission is only slightly perturbed by the electron-donating *tert*-butyl group on the benzene unit of the bzimb ligand (complex **1** versus complex **2**), a clear red-shift in emission is observed for complex **3** (Figure 4) with respect to complex **1**. The electron-donating butoxy group on the benzene unit raises the energy of the HOMO level to a larger extent than that of the LUMO, thus leading to the red-shift in energy (see below).

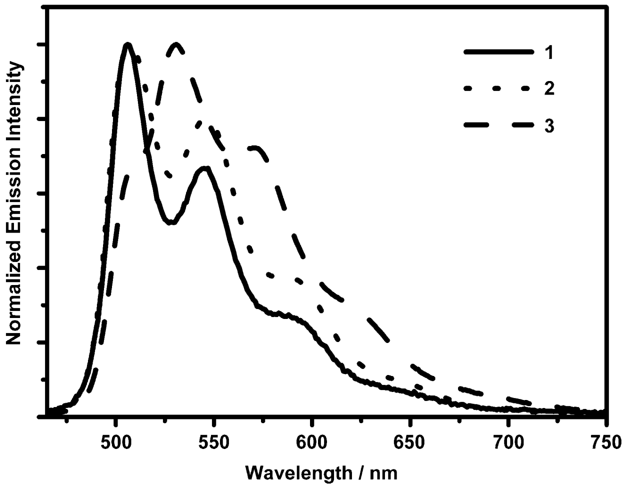

Figure 4. Normalized emission spectra of complexes **1–3** in degassed CH_2Cl_2 at room temperature.

Complexes **4–6** show a vibronic-structured emission band at about 510 nm, which is similar to that of complex **1**. Therefore, this emission most likely originates from the ^{3}IL [π→π*(bzimb)]/MLCT [dπ(Pt)→π*(bzimb)] excited state. Upon increasing the π-conjugation from complex **6** to complex **7**, the vibronic-structured emission band broadens, as shown in Figure 5.

Interestingly, complex **8**, which contains an alkynylpyrenyl moiety, shows two distinct emission bands. In addition to the vibronic-structured emission band at around 507–593 nm, which is derived from the ^{3}IL excited state of the bzimb ligand, a vibronic band is also observed at approximately 659–737 nm (Figure 5). This band is possibly due to the emission from the ^{3}IL π→π*(C≡C–pyrenyl) excited state, as suggested by previous studies on pyrene-containing platinum(II) complexes.[12] This dual emission might result from inefficient coupling between these two excited states.

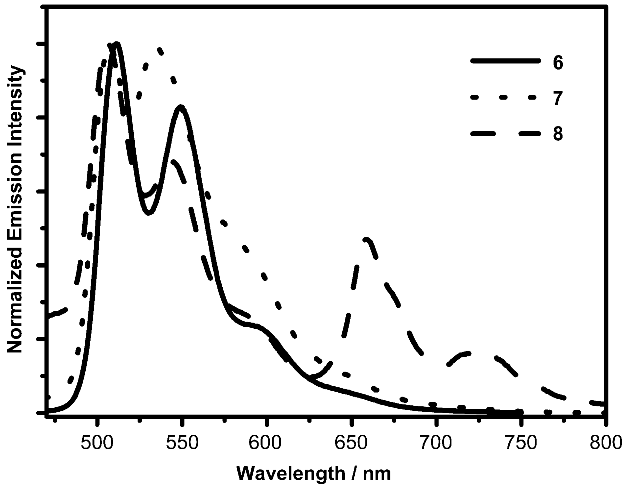

Figure 5. Normalized emission spectra of complexes **6–8** in degassed CH_2Cl_2 at room temperature.

In a butyronitrile glass at 77 K, complexes **4–6** display a well-resolved vibronic-structured emission band at around 490–630 nm, which is assigned to emission from the ^{3}IL [π→π*(bzimb)]/^{3}MLCT [dπ(Pt)→π*(bzimb)] excited state. In complex **8**, apart from the ^{3}IL [π→π*(bzimb)]/^{3}MLCT [dπ(Pt)→π*(bzimb)] vibronic-structured emission band at around 490–564 nm, an additional vibronic-structured band at around 650–776 nm is observed, which is assigned as a ^{3}IL [π→π*(C≡C-pyrenyl)] emission.

Computational studies: DFT and TDDFT calculations were performed for chloro complexes **1–3** and alkynyl complexes **4–8** to gain further insight into the photophysical properties of this series of cyclometalated platinum(II) complexes. In the computational study, model complexes were used (**1′–8′**), in which the long alkyl chains on the nitrogen atoms of the benzimidazolyl groups were replaced by methyl groups.

For chloro complexes **1′–3′**, the S_1 excited state arises from a one-electron excitation from the HOMO to the LUMO. The HOMO is a mixture of the π orbital that is localized on the bzimb ligand and the metal dπ orbital, whilst the LUMO is the π* orbital that is localized on the bzimb ligand (see the Supporting Information, Figure S4). Selected singlet–singlet transitions for complexes **1′–8′** are listed in the Supporting Information, Tables S2–S9. The HOMO energy level increases from complex **1′** to complex **2′** and complex **3′**, in line with the electron-donating ability of the substituents on the benzene unit, that is, butoxy > *tert*-butyl > H. However, the energy of the LUMO level is less influenced by the substituents, because the LUMO has a node on the substituent-bearing carbon atom, which is in agreement with the slight variation in the potential of the reduction waves in our electrochemical studies. The $S_0 \rightarrow S_1$ transition is computed to show a red-shift in energy, in the order **1′** > **2′** > **3′**, which is in good agreement with the trend for the observed lowest-energy absorption band in complexes **1–3** in their UV/Vis absorption spectra and can be assigned as an IL [π–π*(bzimb)]/MLCT [dπ(Pt)→π*(bzimb)] transition.

For alkynyl complexes **4′–6′**, several electronic transitions are computed in the region of the low-energy absorption band. The Supporting Information, Figure S5, shows the molecular orbitals that are involved in these transitions for complex **4′**. The HOMO is mainly the π orbital of the C≡C–R ligand, whereas the HOMO−1 and HOMO−2 are the respective π orbitals of the bzimb ligand mixed with platinum dπ orbitals having Pt–C(bzimb) and Pt–N antibonding character. For the HOMO−1, some mixing of the C≡C π-bonding orbital can be found. The LUMO and LUMO+1 are the π* orbitals of the bzimb ligand. On the basis of the TDDFT calculations, the lower-energy absorption band in complexes

4–6 is mainly due to the IL [π–π*(bzimb)]/LLCT [(C≡C)→π*(bzimb)]/MLCT [dπ→π*(bzimb)] and LLCT [π(C≡C–R)→π*(bzimb)]/MLCT [dπ(Pt)→π*(bzimb)] transitions.

Unlike in complexes **4′**–**6′**, a very intense $S_0 \rightarrow S_2$ transition, which arises from the HOMO→LUMO+1 excitation, is found in complexes **7′** and **8′**. Because the HOMO and LUMO+1 are the respective π and π* orbital of the C≡C–R ligand (see the Supporting Information, Figures S6 and S7), this transition can be assigned as an IL π–π* transition of the C≡C–R ligand. This result is in line with the more intense absorption bands observed for complexes **7** and **8** than for complex **4** in the lower-energy region, thus supporting the involvement of the IL [π–π*(C≡C–R)] transition in the absorption band.

Most of these complexes exhibit strong phosphorescence at room temperature in CH_2Cl_2. To gain more insight into the nature of this emission for this class of complexes, the singlet–triplet transitions were computed for complexes **1′**–**4′**, **7′**, and **8′** by using TDDFT/CPCM with CH_2Cl_2 as the solvent. Because complexes **5** and **6** show similar emission properties to complex **4**, the triplet excited state for complex **4** will be investigated. In the Supporting Information, Tables S10 and S11 list the two lowest-energy singlet–triplet transitions for these complexes. For complexes **1′**–**4′**, the T_1 excited state has ^{3}IL [π–π*(bzimb)]/^{3}MLCT [dπ(Pt)→π*(bzimb)] character. However, the T_1 excited state for complexes **7′** and **8′** has ^{3}IL [π–π*(C≡C–R)] character and the ^{3}IL [π–π*(bzimb)]/^{3}MLCT [dπ(Pt)→π*(bzimb)] excited state becomes the T_2 state. Geometry optimizations of the lowest-energy triplet excited states for these complexes were performed by using the unrestricted Kohn–Sham approach (UPBE0/CPCM). The optimized structures of the triplet excited states for complexes **1′**–**4′** show that the distortion occurs mainly on one of the two benzimidazolyl units and on the central phenyl ring in the bzimb ligand, whereas, for complexes **7′** and **8′**, the distortion is localized on the C≡C–R ligand. Figure 6 shows a plot of the spin densities of the triplet excited state for complexes **1′**, **4′**, **7′**, and **8′**.

The calculated emission wavelengths of the triplet excited states of these complexes, which are approximated from the differences in their solvent-corrected energies at the optimized geometries of the ground and triplet excited states, are listed in Table 3. There is a noticeable red-shift on going from complex **1′** to complex **3′**, which is in line with the observed red-shift in the experiments. This result further supports the tuning of the emission color by modification of the substituents on the benzene unit. A similar emission wavelength of the triplet excited state for complex **4′** to that of complex **1′** is observed, which is in agreement with the experimental findings and further supports the origin of the emission as being derived from the ^{3}IL [π–π*(bzimb)]/^{3}MLCT [dπ(Pt)→π*(bzimb)] excited state.

For complexes **7′** and **8′**, geometry optimizations of the ^{3}IL [π–π*(bzimb)]/^{3}MLCT [dπ(Pt)→π*(bzimb)] triplet excited states were also performed. The emission wavelengths for the ^{3}IL(bzimb)/^{3}MLCT triplet excited states of complexes **7′** (485 nm) and **8′** (483 nm) are similar to that of complex **4′**, whilst the ^{3}IL [π–π*(C≡C–R)] triplet excited states of complexes **7′** and **8′** are computed to be 547 and 679 nm, respectively. As mentioned earlier, two emissions were observed in complex **8**. On the basis of these calculations, as well as the observed trend in the emission bands, the two emissions for complex **8** at around 507–593 and 659–737 nm are assigned to the ^{3}IL(bzimb)/^{3}MLCT and ^{3}IL(C≡C–R) excited states, respectively. Notably, the vibronic-structured emission band for complex **7** at around 507–595 nm is broadened compared to those of complexes **4**–**6**. It is possible that this emission originates from both the ^{3}IL(bzimb)/^{3}MLCT and ^{3}IL [π–π*(C≡C–R)] triplet excited states.

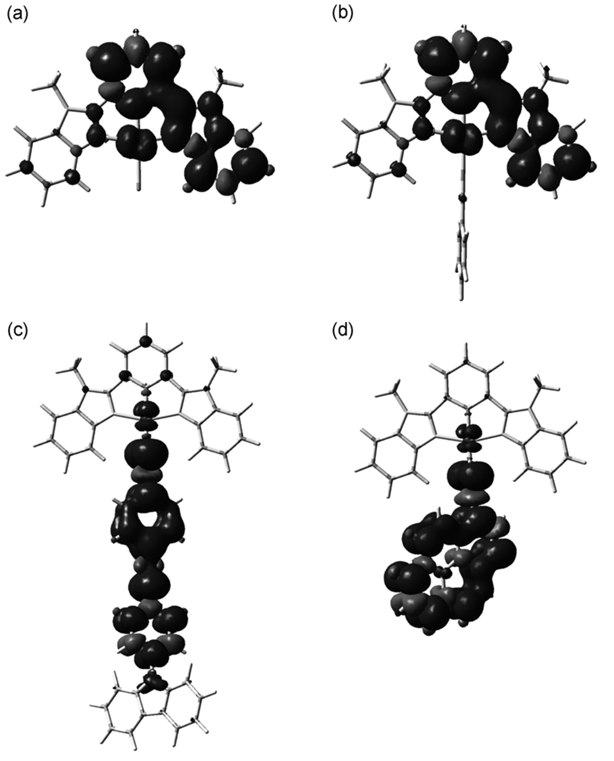

Figure 6. Plot of spin density (isovalue = 0.001) of the lowest-energy triplet-excited states of a) complex **1′**, b) complex **4′**, c) complex **7′**, and d) complex **8′**.

Table 3. Relative energy of the optimized triplet excited states of the model complexes.

Complex	$\Delta E(T_1-S_0)$[a]	Complex	$\Delta E(T_1-S_0)$[a]
1′	487[b]	**4′**	486[b]
2′	491[b]	**7′**	485,[b] 547[c]
3′	530[b]	**8′**	483,[b] 679[c]

[a] Energy difference between the triplet excited states and the ground states at their corresponding optimized geometries in CH_2Cl_2. [b] ^{3}IL(bzimb)/^{3}MLCT excited state. [c] ^{3}IL(C≡C–R) excited state.

Multilayer green OLEDs fabricated by vacuum deposition: As mentioned above, we have recently reported the fabrication of multilayer PHOLEDs by using complex **1** as the emissive layer (EML) and we have demonstrated that they exhibited high current efficiency and EQE (38.9 cd A^{-1} and 11.5 %, respectively).[4a] As an extension of our previous work, complexes **2** and **3** were used as phosphorescent dopant materials to prepare multilayer PHOLEDs by vapor deposition with the configuration of indium tin oxide (ITO)/α-naphthylphenylbiphenyldiamine (NPB; 70 nm)/4,4′,4″-tris(carbazole-9-yl)-triphenylamine (TCTA; 5 nm)/x% Pt^{II}: *N*,*N*′-dicarbazolyl-3,5-benzene (MCP; 30 nm)/3-(4-biphenylyl)-4-phenyl-5-(4-*tert*-butylphenyl)-1,2,4-triazole (TAZ; 5 nm)/bis(2-methyl-8-quinolinato)-4-phenylphenolate)aluminum(III) (BAlq; 30 nm)/LiF/Al with different concentrations of platinum(II) complexes, that is, $x=2$, 4, 6, and 8 %. Similar to the device with complex **1**,[4a] NPB and BAlq were used as hole- and electron-transporting layers, respectively, whilst TCTA and TAZ were used as the carrier-confinement layers. For the devices with **2** and **3**, MCP was used as a host material instead of 4,4′-bis(9-carbazolyl)-2,2′-biphenyl (CBP), because of its higher triplet energy. The Supporting Information, Figure S8, shows the normalized EL spectra of the devices in which complexes **2** and **3** were doped into a MCP layer at a current density of 20 mA cm^{-2}. Both types of devices exhibit a vibronic-structured emission band that is independent of the dopant concentration (see the Supporting Information, Figure S8).[13] Moreover, their EL spectra are similar to their photoluminescence (PL) spectra, thus confirming that they originate from the same ^{3}IL [π–π*] excited state of the cyclometalated bzimb ligand. However, an undesirable blue emission from the adjacent electron-transporting BAlq layer is observed at 480 nm when the dopant concentration of the Pt^{II} complexes is low, which may be due to hole leakage from the emissive layers into the BAlq layer for light emission.

To improve the color purity, devices with dual EMLs were fabricated, in which the platinum(II) complex was doped into both wide-band-gap host materials, that is, MCP and TAZ,[14] to form dual EMLs. In particular, the dopant concentration of the Pt^{II} complexes that were doped into the MCP layer was kept constant (i.e. 8 % for complex **2** and 10 % for complex **3**), whilst different concentrations (i.e. 6, 8, 10, and 12 %) of the Pt^{II} complexes were doped into the TAZ layer. Optimized devices with complexes **2** and **3**

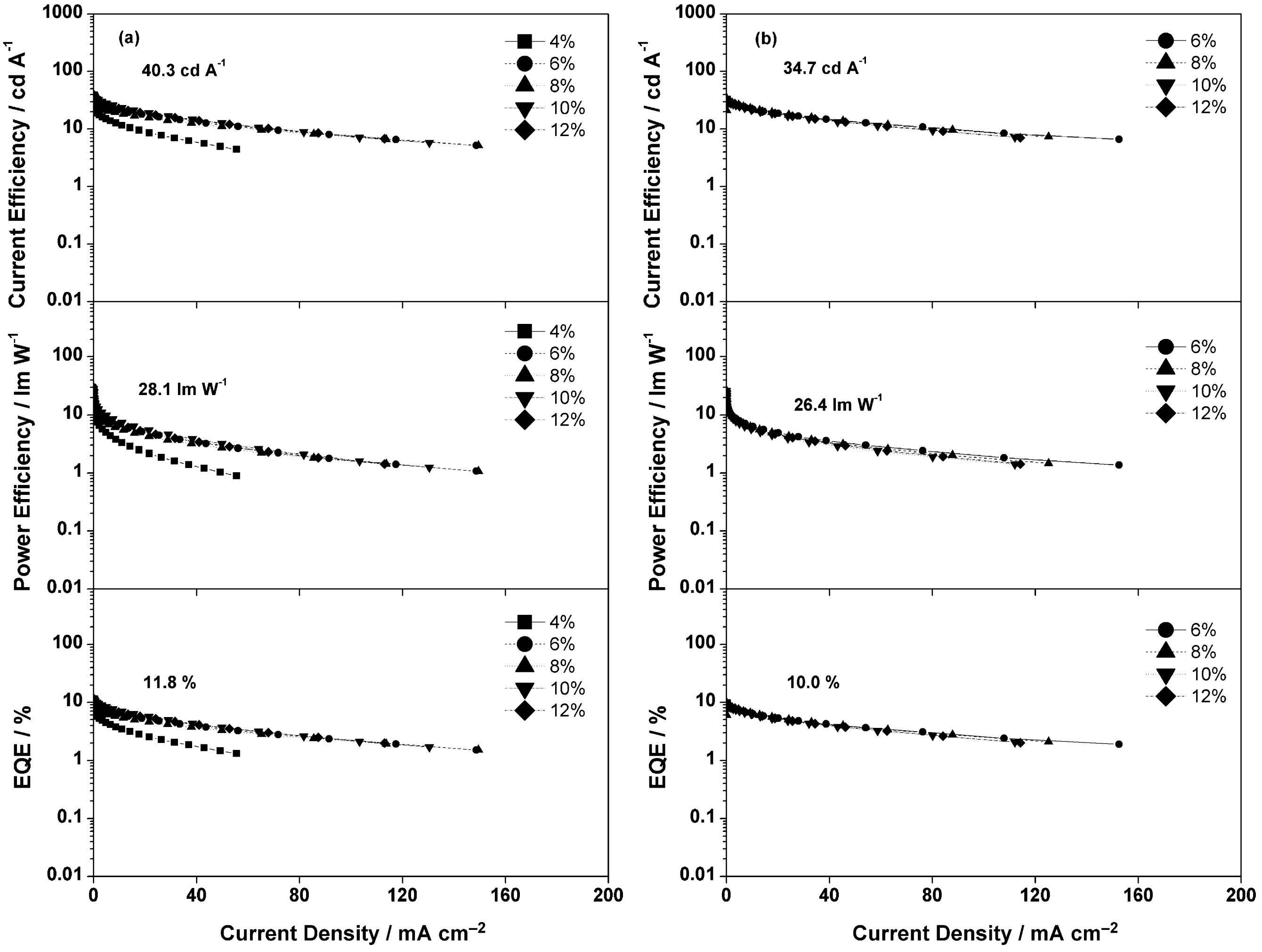

Figure 7. Plots of current efficiency (top), power efficiency (middle), and EQE (bottom) of the dual-EML devices as a function of current density by using a) complex **2** and b) complex **3** as a phosphorescent dopant.

with a single EML show maximum current efficiencies of 15.8 and 23.5 cdA^{-1}, respectively, as well as luminous power efficiencies of 11.1 and 18.4 Lm W^{-1}, respectively. These values correspond to peak EQEs of 5.8% and 6.8% for devices with complexes **2** and **3**, respectively. Upon the introduction of dual EMLs, both the current efficiency and EQE were improved. Devices with complexes **2** and **3** showed maximum current efficiencies of 40.3 and 34.7 cdA^{-1} and EQEs of 11.8% and 10.0%, respectively (Figure 7). More importantly, the EL spectra of all of these devices showed a pure vibronic-structured emission that originated from the Pt^{II} complexes in the absence of any residual emission from BAlq, as shown in Figure 8. Table 4 summarizes the key parameters of devices with single EML and dual EMLs. It is believed that the dual EMLs could effectively confine the triplet excitons within the EML, thereby leading to a suppression of the unwanted BAlq emission. In addition, no significant spectral shift was observed upon increasing the dopant concentration. This result is probably due to a lower tendency of this class of platinum(II) complexes to form aggregates in the solid thin films.[4a]

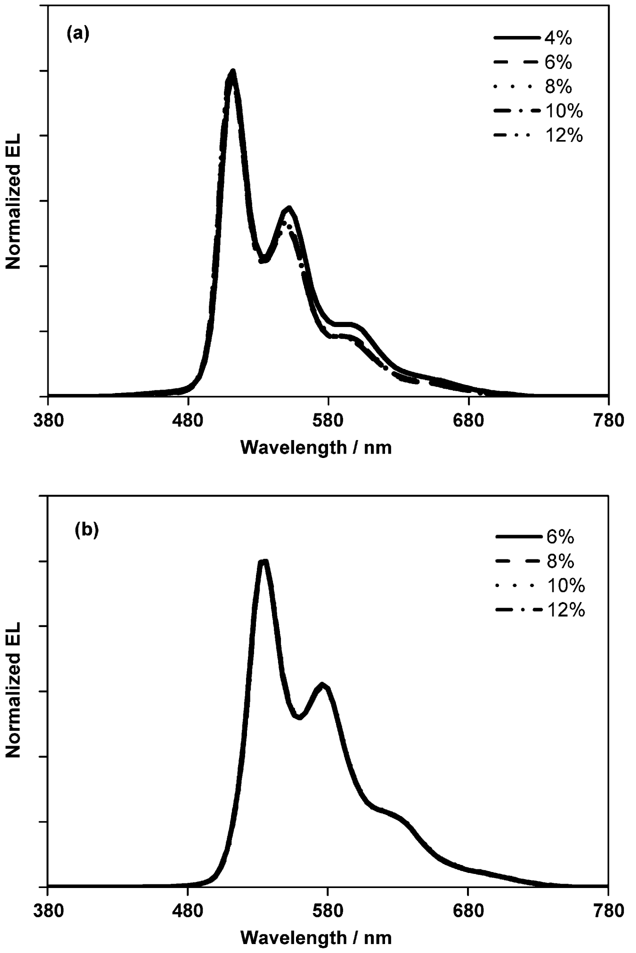

Figure 8. Normalized EL spectra of dual EML devices at a current density of 20 mAcm^{-2} by using a) complex **2** and b) complex **3** as a phosphorescent dopant.

Table 4. Key parameters of devices with a single EML or with dual EMLs.

Complex	Device	Current efficiency [cdA^{-1}]	Power efficiency [lmW^{-1}]	EQE [%]
1[a,b]	single EML	17.8	12.4	5.7
	dual EMLs	38.9	27.2	11.5
2	single EML	15.8	11.1	5.8
	dual EMLs	40.3	28.1	11.8
3	single EML	23.5	18.4	6.8
	dual EMLs	34.7	26.4	10.0

[a] Taken from ref. [4a]. [b] CBP was used as a host material.

Solution-processable multilayer OLEDs: As observed in its PL spectra, complex **8** showed an interesting dual emission (simultaneous green and red emission) in very dilute solutions ([Pt] = 10^{-6} M), and we envisaged that complex **8** would be a good candidate for a white-light-emitting material in a single EML that could be used for the fabrication of WOLEDs. To test this hypothesis, multilayer PHOLEDs with the configuration of ITO/poly(ethylenedioxythiophene):poly(styrene sulfonic acid) (PEDOT:PSS; 70 nm)/ y% **8**:MCP (60 nm)/TAZ (5 nm)/BAlq (30 nm)/LiF/Al (y = 5, 10, and 20%) were fabricated by using a spin-coating technique. Interestingly, the EL is strongly dependent on the concentration of complex **8**. As shown in Figure 9a, at a current density of 60 mAcm^{-2}, white light can be generated by the superposition of two vibronic-structured emission bands in the green and red regions, which are consistent with the PL observation in dilute CH_2Cl_2 at 298 K. Upon increasing the concentration of complex **8**, the EL spectrum is dominated by the vibronic-structured emission band in the red region and the color of light changes from white to yellow and eventually to red at a dopant concentration of 20% (Figure 9b). Table 5 summarizes the key characteristics of this device. Notably, the device with 5% complex **8** gives white-light emission with Commission Internationale de L'Éclairage (CIE) coordinates of (0.35, 0.39), which are very close to those of pure white light (0.33, 0.33). In sharp contrast to other platinum(II) systems that show white-light EL upon dopant aggregation at high concentrations, this class of platinum(II) complexes can give white-light EL emission at low dopant concentrations. To the best of our knowledge, this device represents the first example of white-light EL emission at low concentrations, based on small molecular platinum(II) systems.

Complexes **6** and **7** have also been utilized as phosphorescent dopants in solution-processable OLEDs, in which the device structures were the same as that of complex **8**. Their EL spectra were also found to be independent of the dopant concentration, even up to 20% (Figure 10). Bright-green emission was observed, with vibronic-structured bands at 512, 552, and 600 nm, which corresponded to CIE coordinates of (0.31, 0.55). The lack of distinctive dual-emissive behavior in complexes **6** and **7** led to discrepancies between the emission colors of devices with complex **8** and those

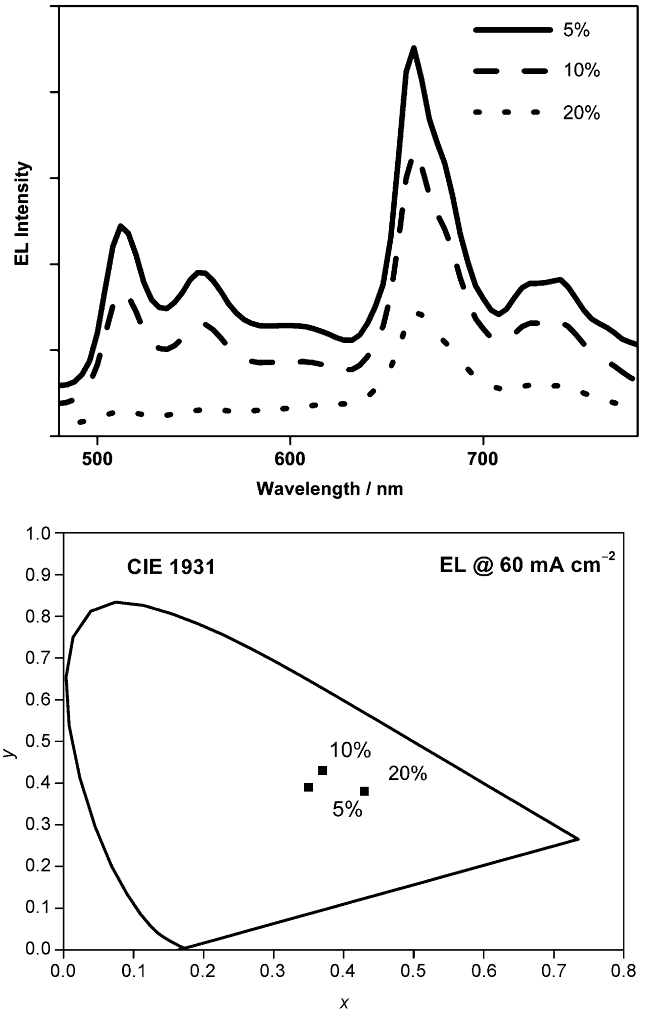

Figure 9. a) EL spectra of devices with complex **8** as a phosphorescent dopant at a current density of 60 mA cm^{-2}. b) Chromaticity diagram, which shows the CIE coordinates of devices at different concentrations.

Table 5. CIE coordinates of devices with complex **8** as an emissive layer.

Dopant concentration [%]	CIE coordinates (*x*,*y*)
5	(0.35, 0.39)
10	(0.37, 0.43)
20	(0.43, 0.38)

with complexes **6** and **7**. On the other hand, the performance of devices that were doped with complexes **6** and **7** was much better than that of devices doped with complex **8**. As shown in Figure 11, the device with complex **6** exhibited a maximum current efficiency of 11.0 cd A^{-1}, which corresponded to an EQE of 3.4 %, whereas the device with complex **7** show a maximum current efficiency of 5.5 cd A^{-1}, which corresponded to an EQE of 1.84 %. The reason for this better performance by doping with complex **6** than with complex **7** may be attributed to reduced hole leakage from the emissive layers into the BAlq layer in devices with complex **6**.

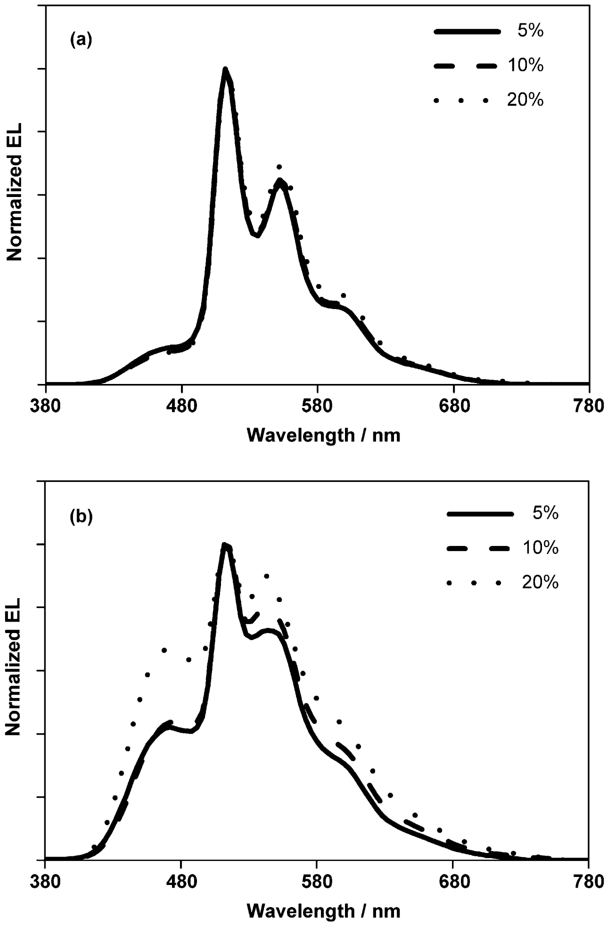

Figure 10. Normalized EL spectra of devices at a current density of 20 mA cm^{-2} by using a) complex **6** and b) complex **7** as a phosphorescent dopant.

Conclusion

In conclusion, a class of [Pt(bzimb)Cl] complexes with tunable emission color has been synthesized and their photophysical properties have been characterized. By varying the functional groups on the benzene unit in chloro complexes [Pt(R-bzimb)Cl], the emission color can be readily tuned. Moreover, by incorporating an alkynyl ligand into complexes [Pt(bzimb)(C≡C−R)], an enhancement in PL quantum efficiency can be achieved. Multilayer PHOLEDs have been fabricated based on these platinum(II) complexes. Devices with complex **2** demonstrated high current efficiencies and EQEs of up to 40.3 cd A^{-1} and 11.8 %, respectively, whilst solution-processable devices with complexes **6** and **7** exhibited EQEs of 3.4 % and 1.8 %, respectively. Interestingly, white light can be obtained by using complex **8** as a phosphorescent dopant in solution-processable PHOLEDs. Dual emission can be observed in devices with complex **8**, in which green and red emissions originate from ^{3}IL-(bzimb)/^{3}MLCT and ^{3}IL(C≡C−R)/^{3}MLCT excited states, respectively. This interesting observation may be helpful for providing new insight into the development of PHOLEDs

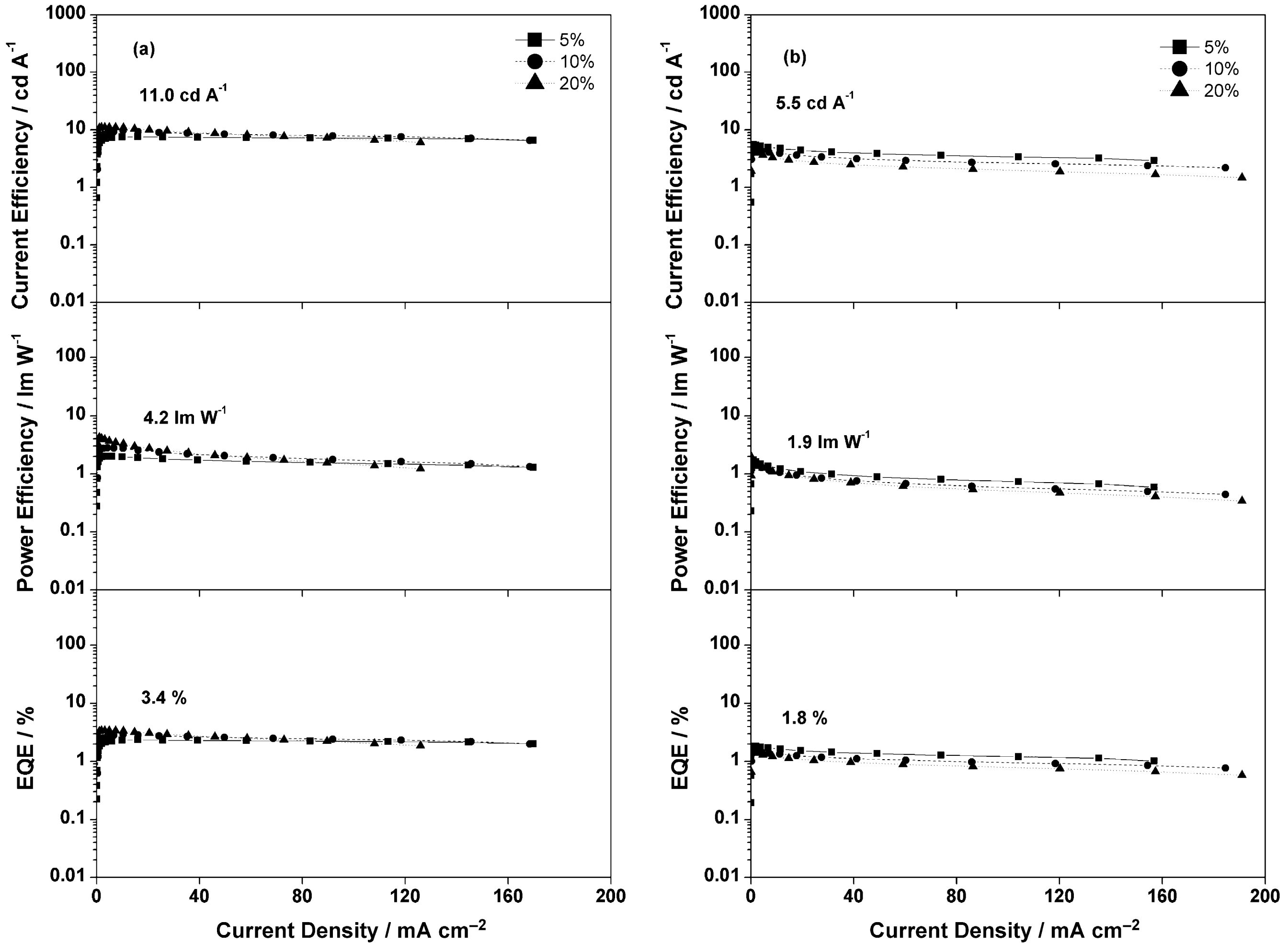

Figure 11. Plots of current efficiency (top), power efficiency (middle), and EQE (bottom) of the devices as a function of current density by using a) complex **6** and b) complex **7** as a phosphorescent dopant.

and WOLEDs. We envisage that, with a suitable choice of π-conjugated alkynyl ligands, multiple emissions may result that could generate white light from a single-molecule emissive material.

Experimental Section

Materials: Sodium hydroxide, 1-bromobutane, 1-ethynylpyrene, and phenylacetylene were obtained from Aldrich. 9-(4-Ethynylphenyl)carbazole,[15a] 4-ethynyl-*N*,*N*-diphenylaniline,[15b] ((4-bromophenyl)ethynyl)trimethylsilane,[15c] 1,3-bis(benzimidazol-2′-yl)benzene (bzimb),[4a] complex **1**,[4a] and complex **6**[4g] were synthesized according to literature procedures. The chloroplatinum(II) precursor complexes were synthesized according to a modified literature procedures for the synthesis of chloroplastinum(II)–2,6-bis(benzimidazol-2′-yl)pyridine (bzimpy) complexes.[9] All solvents were purified and distilled by using standard procedures before use. All other reagents were of analytical grade and were used as received.

Synthesis of 9-(4-((4-((trimethylsilyl)ethynyl)phenyl)ethynyl)phenyl)-9*H*-carbazole: 9-(4-Ethynylphenyl)carbazole (0.65 g, 2.4 mmol), CuI (0.02 g, 0.1 mmol), ((4-bromophenyl)ethynyl)trimethylsilane (1.23 g, 4.9 mmol), and *trans*-dichlorobis(triphenylphosphine)palladium(II) (0.08, 0.1 mmol) were added to distilled triethylamine (60 mL) under a nitrogen atmosphere and the mixture was heated at reflux for 1 day. After the removal of the solvent, the solid was purified by column chromatography on silica gel by using *n*-hexane/CH_2Cl_2 (4:1 v/v) to obtain the product as a pure white solid. Yield: 0.47 g (45 % yield). ^{1}H NMR (400 MHz, $CDCl_3$): δ = 0.33 (s, 9H; CH_3), 7.30 (t, J=7.8 Hz, 2H; carbazole H), 7.46 (m, 8H; benzene H), 7.58 (d, J=8.5 Hz, 2H; carbazole H), 7.75 (d, J=8.5 Hz, 2H; carbazole H), 8.15 (d, J=7.8 Hz, 2H; carbazole H); MS (FAB, positive-ion mode): m/z 440 $[M+H]^+$; HRMS (EI, positive-ion mode): m/z calcd for $C_{31}H_{25}N_{28}Si$: 439.1751; found: 439.1751.

Synthesis of complex 2: The product was synthesized according to a modified procedure for the synthesis of [Pt(*n*BuBzimb)Cl],[4a] except that 1,3-bis(*N*-butylbenzimidazol-2′-yl)-4-*tert*-butylbenzene (0.5 g, 1.0 mmol) was used in the place of 1,3-bis(*N*-butylbenzimidazol-2′-yl)benzene. Yield: 0.2 g (40 %); ^{1}H NMR (400 MHz, $CDCl_3$): δ=0.98 (t, J=7.6 Hz, 6H; CH_3), 1.49 (m, 4H; CH_2), 1.58 (s, 9H; CH_3), 1.87 (m, 4H; CH_2), 4.48 (t, J=7.6 Hz, 4H; CH_2), 7.02 (d, J=8.0 Hz, 2H; benzimidazolyl H), 7.25 (m, 4H; benzimidazolyl H), 7.46 (s, 2H; C_6H_2), 8.85 (d, J=8.0 Hz, 2H; benzimidazolyl H); MS (FAB, positive-ion mode): m/z 709 $[M+H]^+$; elemental analysis calcd (%) for $C_{32}H_{37}ClN_4Pt$: C 54.27, H 5.27, N 7.91; found: C 54.19, H 5.35, N 7.84.

Synthesis of complex 3: The product was synthesized according to a modified procedure for the synthesis of [Pt(*n*BuBzimb)Cl],[4a] except 1,3-bis(*N*-butylbenzimidazol-2′-yl)-5-butoxybenzene (0.15 g, 0.3 mmol) was used in place of 1,3-bis(*N*-butylbenzimidazol-2′-yl)benzene. Yield: 0.04 g (33 %); ^{1}H NMR (400 MHz, CDCl$_3$): δ = 0.96 (m, 9H; CH$_3$), 1.46 (m, 6H; CH$_2$), 1.60 (m, 2H; CH$_2$), 1.88 (m, 4H; CH$_2$), 3.90 (t, J = 6.4 Hz, 2H; O–CH$_2$), 4.51 (t, J = 7.3 Hz, 4H; CH$_2$), 6.97 (s, 2H; benzimidazolyl H), 7.14 (d, J = 8.0 Hz, 2H; benzimidazolyl H), 7.30 (m, 4H; benzimidazolyl H), 8.95 (d, J = 8.0 Hz, 2H; benzimidazolyl H); MS (FAB, positive-ion mode): *m*/*z* 725 [*M*+H]$^+$; elemental analysis calcd (%) for $C_{32}H_{38}N_4Pt{\cdot}H_2O$: C 52.85, H 5.54, N 7.70; found: C 52.91, H 5.15, N 7.71.

Synthesis of complex 4: The product was synthesized according to a similar procedure for the synthesis of complex **6**.[4g] A mixture of phenylacetylene (0.1 mL, 0.91 mmol) and sodium hydroxide (0.02 g, 0.5 mmol) was stirred in MeOH (10 mL) at RT. After 30 min, a solution of [Pt(*n*BuBzimb)Cl] (0.1 g, 0.15 mmol) in CH$_2$Cl$_2$ was added and the mixture was stirred under heating at 50 °C for 2 days. After filtration, the yellow precipitate was washed with water, MeOH, and Et$_2$O. Slow diffusion of Et$_2$O vapor into a solution of the product in CH$_2$Cl$_2$ gave complex **4** as a yellow powder. Yield: 0.07 g (64 %); ^{1}H NMR (400 MHz, CDCl$_3$): δ = 0.98 (t, J = 7.4 Hz, 6H; CH$_3$), 1.47 (m, 4H; CH$_2$), 1.94 (m, 4H; CH$_2$), 4.56 (t, J = 7.4 Hz, 4H; CH$_2$), 7.31 (m, 9H; benzimidazolyl H and C$_6$H$_4$), 7.53 (d, J = 8.0 Hz, 2H; benzimidazolyl H), 7.70 (d, J = 7.1 Hz, 2H; C$_6$H$_4$), 9.05 (d, J = 8.0 Hz, 2H; benzimidazolyl H); IR (KBr): $\tilde{\nu}$ = 2089 cm^{-1} (w, C≡C); MS (FAB, positive-ion mode): *m*/*z* 719 [*M*+H]$^+$; elemental analysis calcd (%) for $C_{36}H_{34}N_4Pt$: C 60.24, H 4.77, N 7.81; found: C 60.33, H 4.88, N 7.81.

Synthesis of complex 5: The product was synthesized according to a similar procedure for the synthesis of complex **4**, except that 4-ethynyl-*N*,*N*-diphenylaniline (0.25 g, 0.6 mmol) was used in place of phenylacetylene. Yield: 0.09 g (66 %); ^{1}H NMR (400 MHz, CDCl$_3$): δ = 0.99 (t, J = 7.4 Hz, 6H; CH$_3$), 1.52 (m, 4H; CH$_2$), 1.98 (m, 4H; CH$_2$), 4.60 (t, J = 7.4 Hz, 4H; CH$_2$), 7.00 (t, J = 7.5 Hz, 2H; triphenylamine), 7.09 (d, J = 8.6 Hz, 2H; triphenylamine), 7.17 (d, J = 7.5 Hz, 4H; triphenylamine), 7.27 (m, 5H; benzimidazolyl H), 7.33 (m, 4H; benzimidazolyl H), 7.40 (m, 2H; triphenylamine), 7.58 (t, J = 7.5 Hz, 4H; triphenylamine), 9.13 (d, J = 7.9 Hz, 2H; benzimidazolyl H); IR (KBr): $\tilde{\nu}$ = 2083 cm^{-1} (w, C≡C); MS (FAB, positive-ion mode): *m*/*z* 886 [*M*+H]$^+$; elemental analysis calcd (%) for $C_{48}H_{43}N_5Pt{\cdot}0.5\,H_2O$: C 64.49, H 4.96, N 7.83; found: C 64.62, H 4.91, N 7.85.

Synthesis of complex 7: The product was synthesized according to a similar procedure for the synthesis of complex **4**, except that 9-(4-((4-((trimethylsilyl)ethynyl)phenyl)ethynyl)phenyl)-9*H*-carbazole (0.13 g, 0.3 mmol) was used in place of phenylacetylene. Yield: 0.08 g (53 %); ^{1}H NMR (400 MHz, CDCl$_3$): δ = 0.98 (t, J = 7.4 Hz, 6H; CH$_3$), 1.47 (m, 4H; CH$_2$), 1.93 (m, 4H; CH$_2$), 4.56 (t, J = 7.4 Hz, 4H; CH$_2$), 7.22 (m, 3H; carbazole H and C$_6$H$_4$–C≡C–C$_6$H$_4$), 7.30 (m, 4H; C$_6$H$_4$–C≡C–C$_6$H$_4$ and benzimidazolyl H), 7.38 (t, J = 8.0 Hz, 2H; carbazole H), 7.47 (m, 6H; benzimidazolyl and carbazole H), 7.60 (t, J = 8.0 Hz, 4H; benzimidazolyl H), 7.69 (d, J = 8.0 Hz, 2H; carbazole H), 7.80 (d, J = 8.0 Hz, 2H; carbazole H), 8.16 (d, J = 8.0 Hz, 2H; C$_6$H$_4$–C≡C–C$_6$H$_4$), 8.97 (d, J = 8.0 Hz, 2H; benzimidazolyl H); IR (KBr): $\tilde{\nu}$ = 2077 cm^{-1} (w, C≡C); MS (FAB, positive-ion mode): *m*/*z* 984 [*M*+H]$^+$; elemental analysis calcd (%) for $C_{56}H_{45}N_5Pt{\cdot}0.5\,H_2O$: C 67.79, H 4.67, N 7.06; found: C 67.50, H 4.57, N 6.92.

Synthesis of complex 8: The product was synthesized according to a similar procedure for the synthesis of complex **4**, except that 1-ethynylpyrene (0.1 g, 0.3 mmol) was used in place of phenylacetylene. Yield: 0.1 g (77 %); ^{1}H NMR (400 MHz, CDCl$_3$): δ = 1.02 (t, J = 7.4 Hz, 6H; CH$_3$), 1.55 (m, 4H; CH$_2$), 2.02 (m, 4H; CH$_2$), 4.64 (t, J = 7.4 Hz, 4H; CH$_2$), 7.34 (m, 7H; benzimidazolyl H), 7.64 (d, J = 7.8 Hz, 2H; benzimidazolyl H), 8.1 (m, 7H; pyrene H), 8.39 (d, J = 7.9 Hz, 1H; pyrene H), 9.27 (m, 3H; pyrene and benzimidazolyl H); IR (KBr): $\tilde{\nu}$ = 2066 cm^{-1} (w, C≡C); MS (FAB, positive-ion mode): *m*/*z* 845 [*M*+H]$^+$; elemental analysis calcd (%) for $C_{46}H_{40}N_4Pt{\cdot}0.5(CH_3CN){\cdot}0.5\,C_6H_{14}$: C 66.17, H 5.08, N 6.95; found: C 66.48, H 4.76, N 6.91.

Physical measurements and instrumentation: ^{1}H NMR spectroscopy was performed on a Bruker AVANCE 400 (400 MHz) Fourier-transform NMR spectrometer; chemical shifts are reported relative to tetramethylsilane. Positive-ion FAB MS was performed on a Thermo Scientific DFS high-resolution magnetic sector mass spectrometer. IR spectroscopy was performed on KBr disks on a Bio-Rad FTS-7 FTIR spectrometer (4000–400 cm^{-1}). Elemental analysis of the new complexes was performed on a Flash EA 1112 elemental analyzer at the Institute of Chemistry, the Chinese Academy of Sciences.

Electronic absorption spectroscopy was performed on a Hewlett–Packard 8452A diode-array spectrophotometer. The concentration of the samples for the electronic absorption measurements were typically within the range 2×10^{-4} to 1×10^{-6} mol dm^{-3}. Steady-state excitation and emission spectroscopy were performed on a Spex Fluorolog-2 Model F111 fluorescence spectrofluorimeter at RT and 77 K. Solid-state photophysical studies were performed on solid samples inside a quartz tube that was placed inside a quartz-walled Dewar flask. Similarly, measurements of a butyronitrile glass or solid-state sample at 77 K were performed by adding liquid nitrogen into the optical Dewar flask. The concentration of the complexes in butyronitrile glass for the emission measurements was typically of the order $\times10^{-6}$ mol dm^{-3}. For the photophysical studies, all of the solutions were degassed on a high-vacuum line in a two-compartment cell that consisted of a Pyrex bulb (10 mL) and a quartz cuvette (path length: 1 cm) and was sealed from the atmosphere by a Bibby Rotaflo HP6 Teflon stopper. The solutions were rigorously degassed by at least four successive freeze/pump/thaw cycles. Emission-lifetime measurements were performed by using a conventional laser system. The concentrations of the complexes in solution for the lifetime measurements were typically about 2×10^{-5} mol dm^{-3}. The excitation source was a 355 nm output (third harmonic) of a Spectra-Physics Quanta-Ray Q-switched GCR-150–10 pulsed Nd-YAG laser. Luminescence-decay signals were detected on a Hamamatsu R928 PMT, recorded on a Tektronix Model TDS-620A (500 MHz, 2GS/s) digital oscilloscope, and analyzed by using a program for the exponential fits.

Cyclic voltammetry was performed on a CHI 620A (CH Instruments, Inc.) electrochemical analyzer. Electrochemical measurements were performed at RT in CH$_2$Cl$_2$ with 0.1 mol dm^{-3} *n*Bu$_4$NPF$_6$ (TBAH) as the supporting electrolyte. The reference electrode was an Ag/AgNO$_3$ (0.1 mol dm^{-3} in MeCN) electrode, the working electrode was a glassy carbon electrode (CH Instruments), and Pt wire was used as the counter electrode. The surface of the working electrode was polished with a 1 μm alumina slurry (Linde) on a microcloth (Buehler) and then with a 0.3 μm alumina slurry. Then, the surface was rinsed with ultra-pure deionized water and sonicated in a beaker that contained ultra-pure water for 5 min. The polishing and sonication steps were repeated twice and, finally, the working electrode was rinsed under a stream of ultra-pure deionized water. The ferrocenium/ferrocene couple (FeCp$_2^+$/FeCp$_2^0$) was used as an internal reference. All solutions for the electrochemical studies were deaerated with pre-purified Ar gas prior to the measurements.

X-ray crystal-structure determination: Single crystals of complex **7** that were suitable for X-ray diffraction studies were grown by layering Et$_2$O onto a concentrated solution of the complex in CH$_2$Cl$_2$. The X-ray diffraction data were collected on a Bruker *APEX II* CCD detector with graphite-monochromated Mo$_{K\alpha}$ radiation (λ = 0.71073 Å). The raw frame data were integrated by using the SAINT[16] program. Multi-scan SADABS[17] was applied during the absorption correction. The structure was solved by using heavy-atom Patterson methods[18] and expanded by using Fourier techniques. Full-matrix least-squares refinement on F^2 was used in the structure refinement. The positions of the H atoms were calculated on the basis of the riding mode with thermal parameters equal to 1.2 times that of the associated C atoms and these positions participated in the calculation of the final *R* indices. In the final stage of least-squares refinement, all non-hydrogen atoms were refined anisotropically. Crystallographic and structural refinement data are given in the Supporting Information, Table S1.

CCDC-880903 (**7**) contains the supplementary crystallographic data for this paper. These data can be obtained free of charge from The Cambridge Crystallographic Data Centre via www.ccdc.cam.ac.uk/data_request/cif.

Computational details: Calculations were performed by using the Gaussian 09 software package.[19] The ground-state geometries of model complexes **1′**–**8′** were fully optimized in CH$_2$Cl$_2$ by using DFT calculations with the hybrid Perdew, Burke, and Ernzerhof functional (PBE0)[20] in conjunction with the conductor-like polarizable continuum model (CPCM).[21] On the basis of the ground-state-optimized geometries, the TDDFT[22] method at the same level associated with the CPCM (CH_2Cl_2) was employed to compute the singlet–singlet and singlet–triplet transitions. To gain more insight into the emissive states, geometry optimizations of the triplet excited states were performed by using the unrestricted UPBE0/CPCM (CH_2Cl_2) method. The calculated emission wavelength of the triplet excited state for the complexes was approximated from the difference in the solvent-corrected energies at the optimized geometries of the ground and triplet excited states. Vibrational frequency calculations were performed for all stationary points to verify that each was a minimum (NIMAG = 0) on the potential-energy surface. For all of the calculations, the Stuttgart effective core potentials (ECPs) and the associated basis set were applied to describe Pt[23] with f-type polarization functions ($\zeta = 0.993$),[24] whereas, for all other atoms, the 6–31G(d,p) basis set[25] was used.

Fabrication and characterization of the PHOLEDs: The PHOLEDs were fabricated on patterned ITO-coated glass substrates with a sheet resistance of 30 Ω/sq. The substrates were cleaned with Decon 90, rinsed with de-ionized water, dried in an oven, and treated in an ultraviolet ozone chamber. For the PHOLEDs, NPB (thickness: 70 nm) was used as the hole-transporting layer and TCTA (thickness: 5 nm) was used as the carrier-confinement layer. An emissive layer (thickness: 30 nm) that consisted of Pt complexes doped into the MCP layer with different dopant concentrations was prepared by thermal co-deposition. For solution-processed OLEDs, PEDOT:PSS (thickness: 70 nm) was spin-coated onto the ITO-coated glass substrates as a hole-transporting layer. After that, the emissive layer was formed by mixing the Pt complexes with MCP to prepare $10\,mg\,cm^{-3}$ solutions in $CHCl_3$ and spin-coating onto the PEDOT:PSS layer to give uniform thin films with a thickness of 60 nm. All devices were completed by depositing TAZ (thickness: 5 nm) and BAlq (thickness: 30 nm) as hole-blocking and electron-transporting layers, respectively; LiF/Al was used as the metal cathode. All films were sequentially deposited at a rate of $0.1–0.2\,nm\,s^{-1}$ without a vacuum break. A shadow mask was used to define the cathode and to make four $0.1\,cm^2$ devices on each substrate. Current-density–voltage–luminance characteristics and EL spectra were measured simultaneously with a programmable Keithley model 2400 power source and a Photoresearch PR650 spectrometer.

Supporting information: The Supporting Information, Table S1, lists the X-ray crystallographic data for complex **7**. Tables S2–S9 list selected singlet–singlet transitions of model complexes **1′**–**8′**, which were computed by using TDDFT/CPCM (CH_2Cl_2). Tables S10 and S11 list the first two lowest-lying triplet excited states, as computed by using TDDFT/CPCM (CH_2Cl_2), for complexes **1′**–**4′**, **7′**, and **8′**. The Supporting Information, Figure S1, shows the crystal-packing diagram of complex **7**. Figure S2 shows the cyclic voltammogram of complex **5**. Figure S3 shows electronic absorption spectra of complexes **4**, **6**, and **8**. Figures S4–S7 show spatial plots of selected molecular orbitals of complexes **1′**, **4′**, **7′**, and **8′**. Figure S8 shows normalized EL spectra of single EML devices with complexes **2** and **3**, as well as Cartesian coordinates of their optimized geometries.

Acknowledgements

V.W.-W.Y. acknowledges support from The University of Hong Kong and the URC Strategic Research Theme on Molecular Materials. This work has been supported by a grant from the Theme-Based Research Scheme (TBRS) of the Research Grants Council of the Hong Kong Special Administrative Region, China (Project No. T23–713/11). E.S.-H.L. acknowledges the receipt of a Postgraduate Studentship and A.Y.-Y.T. acknowledges the receipt of a University Postdoctoral Fellowship, both from The University of Hong Kong. We are grateful to Dr. L. Szeto for her assistance in X-ray crystal-structure data collection and determination and to the Computer Center of The University of Hong Kong for providing computational resources.

---

[1] a) S. R. Forrest, *Nature* **2004**, *428*, 911; b) B. W. D'Andrade, S. R. Forrest, *Adv. Mater.* **2004**, *16*, 1585; c) B. W. D'Andrade, *Nat. Photonics* **2007**, *1*, 33.

[2] a) M. A. Baldo, D. F. O'Brien, Y. You, A. Shoustikovm, S. Sibley, M. E. Thompson, S. R. Forrest, *Nature* **1998**, *395*, 151; b) M. A. Baldo, S. Lamansky, M. E. Thompson, S. R. Forrest, *Appl. Phys. Lett.* **1999**, *75*, 4; c) M. A. Baldo, M. E. Thompson, S. R. Forrest, *Nature* **2000**, *403*, 750; d) G. He, M. Pfeiffer, K. Leo, M. Hofmann, J. Birnstock, R. Pudzich, J. Salbeck, *Appl. Phys. Lett.* **2004**, *85*, 3911.

[3] M. Cocchi, J. Kalinowski, L. Murphy, J. A. G. Williams, V. Fattori, *Org. Electron.* **2010**, *11*, 388.

[4] a) A. Y.-Y. Tam, D. P.-K. Tsang, M.-Y. Chan, N. Y. Zhu, V. W.-W. Yam, *Chem. Commun.* **2011**, *47*, 3383; b) S. C. F. Kui, I. H. T. Sham, C. C. C. Cheung, C.-W. Ma, B. Yan, N. Zhu, C.-M. Che, W.-F. Fu, *Chem. Eur. J.* **2007**, *13*, 417; c) W. Lu, B.-X. Mi, M. C. W. Chan, Z. Hui, C.-M. Che, N. Y. Zhu, S.-T. Lee, *J. Am. Chem. Soc.* **2004**, *126*, 4958; d) Z. Wang, E, Turner, V. Mahoney, S. Madakuni, T. Groy, J. Li, *Inorg. Chem.* **2010**, *49*, 11276; e) S. J. Farley, D. L. Rochester, A. L. Thompson, J. A. K. Howard, J. A. G. Williams, *Inorg. Chem.* **2005**, *44*, 9690; f) D. L. Rochester, S. Develay, S. Zális, J. A. G. Williams, *Dalton Trans.* **2009**, 1728; g) E. S. H. Lam, A. Y.-Y. Tam, W. H. Lam, K. M.-C. Wong, N. Y. Zhu, V. W.-W. Yam, *Dalton Trans.* **2012**, *41*, 8773.

[5] a) R. F. Carina, A. F. Williams, G. Bernardinelli, *J. Organomet. Chem.* **1997**, *548*, 45; b) T. Yutaka, S. Obara, S. Ogawa, K. Nozaki, N. Ikeda, T. Ohno, Y. Ishii, K. Sakai, M. Haga, *Inorg. Chem.* **2005**, *44*, 4737.

[6] a) B. P. Yan, C. C. C. Cheung, S. C. F. Kui, H.-F. Xiang, V. A. L. Roy, S.-J. Xu, C.-M. Che, *Adv. Mater.* **2007**, *19*, 3599; b) Z. Shen, P. E. Burrows, V. Bulović, S. R. Forrest, M. E. Thompson, *Science* **1997**, *276*, 2009.

[7] a) E. L. Williams, K. Haavisto, J. Li, G. E. Jabbour, *Adv. Mater.* **2007**, *19*, 197; b) X. Yang, Z. Wang, S. Madakuni, G. E. Jabbour, *Adv. Mater.* **2008**, *20*, 2405; c) V. Adamovich, J. Brooks, A. Tamayo, A. M. Alexander, P. I. Djurovich, B. W. D′Andrade, C. Adachi, S. R. Forrest, M. E. Thompson, *New J. Chem.* **2002**, *26*, 1171.

[8] H. J. Bolink, F. De Angelis, E. Baranoff, C. Klein, S. Fantacci, E. Coronado, M. Sessolo, K. Kalyanasundaram, M. Grätzel, Md. K. Nazeeruddin, *Chem. Commun.* **2009**, 4672.

[9] A. Y.-Y. Tam, W. H. Lam, K. M.-C. Wong, N. Zhu, V. W.-W. Yam, *Chem. Eur. J.* **2008**, *14*, 4562.

[10] a) O. Yurchenko, D. Freytag, L. zur Borg, R. Zentel, J. Heinze, S. Ludwigs, *J. Phys. Chem. B* **2012**, *116*, 30; b) S. C. Jones, V. Coropceanu, S. Barlow, T. Kinnibrugh, T. Timofeeva, J. L. Brédas, S. R. Marder, *J. Am. Chem. Soc.* **2004**, *126*, 11782.

[11] a) B. R. Hsieh, M. H. Litt, *Macromolecules* **1986**, *19*, 521; b) Z. P. Zhang, B. K. Jin, Y. P. Tian, S. J. Wang, *Chin. Chem. Lett.* **2005**, *16*, 1621; c) M. Ates, K. Yilmaz, A. Shahryari, S. Omanovic, A. S. Sarac, *IEEE Sens. J.* **2008**, *8*, 1628.

[12] Q. Wang, F. Xiong, F. Morlet-Savary, S. Li, Y. Li, J.-P. Fouassier, G. Q. Yang, *J. Photochem. Photobiol. A* **2008**, *194*, 230.

[13] Z. He, W.-Y. Wong, H.-S. Kwok, Z. Lin, *Inorg. Chem.* **2006**, *45*, 10922.

[14] H. Sasabe, E. Gonmori, T. Chiba, Y. J. Li, D. Tanaka, S. J. Su, T. Takeda, Y. J. Pu, K. Nakayama, J. Kido, *Chem. Mater.* **2008**, *20*, 5951.

[15] a) F. Sanda, T. Kawaguchi, T. Masuda, *Macromolecules* **2003**, *36*, 2224; b) S. Ch. Suh, M. Ch. Suh, S. Ch. Shim, *Macromol. Chem. Phys.* **1999**, *200*, 1991; c) R. J. Rahaim, J. T. Shaw, *J. Org. Chem.* **2008**, *73*, 2912.

[16] *SAINT+, SAX area detector integration program*, version 7.34 A; Bruker AXS, Inc., Madison.

[17] G. M. Sheldrick, *SADABS, Program for empirical absorption correction of area-detector data*, Universität Göttingen, Germany, **2008**.

[18] P. T. Beurskens, G. Admiraal, G. Beurskens, W. P. Bosman, R. de Gelder, R, Israel, J. M. M. Smits, *The DIRDIF-99 program system, Technical Report of the Crystallography Laboratory*, University of Nijmegen, The Netherlands, **1999**.

[19] Gaussian 09 (Revision C.01), M. J. Frisch, G. W. Trucks, H. B. Schlegel, G. E. Scuseria, M. A. Robb, J. R. Cheeseman, G. Scalmani, V. Barone, B. Mennucci, G. A. Petersson, H. Nakatsuji, M. Caricato, X. Li, H. P. Hratchian, A. F. Izmaylov, J. Bloino, G. Zheng, J. L. Sonnenberg, M. Hada, M. Ehara, K. Toyota, R. Fukuda, J. Hasegawa, M. Ishida, T. Nakajima, Y. Honda, O. Kitao, H. Nakai, T. Vreven, J. A. Montgomery, Jr., J. E. Peralta, F. Ogliaro, M. Bearpark, J. J. Heyd, E. Brothers, K. N. Kudin, V. N. Staroverov, T. Keith, R. Kobayashi, J. Normand, K. Raghavachari, A. Rendell, J. C. Burant, S. S. Iyengar, J. Tomasi, M. Cossi, N. Rega, J. M. Millam, M. Klene, J. E. Knox, J. B. Cross, V. Bakken, C. Adamo, J. Jaramillo, R. Gomperts, R. E. Stratmann, O. Yazyev, A. J. Austin, R. Cammi, C. Pomelli, J. W. Ochterski, R. L. Martin, K. Morokuma, V. G. Zakrzewski, G. A. Voth, P. Salvador, J. J. Dannenberg, S. Dapprich, A. D. Daniels, Ö. Farkas, J. B. Foresman, J. V. Ortiz, J. Cioslowski, D. J. Fox, Gaussian, Inc., Wallingford CT, **2010**.

[20] a) J. P. Perdew, K. Burke, M. Ernzerhof, *Phys. Rev. Lett.* **1996**, *77*, 3865; b) J. P. Perdew, K. Burke, M. Ernzerhof, *Phys. Rev. Lett.* **1997**, *78*, 1396; c) C. Adamo, V. Barone, *J. Chem. Phys.* **1999**, *110*, 6158.

[21] a) V. Barone, M. Cossi, *J. Phys. Chem. A* **1998**, *102*, 1995; b) M. Cossi, N. Rega, G. Scalmani, V. Barone, *J. Comput. Chem.* **2003**, *24*, 669.

[22] a) R. E. Stratmann, G. E. Scuseria, M. J. Frisch, *J. Chem. Phys.* **1998**, *109*, 8218; b) R. Bauernschmitt, R. Ahlrichs, *Chem. Phys. Lett.* **1996**, *256*, 454; c) M. E. Casida, C. Jamorski, K. C. Casida, D. R. Salahub, *J. Chem. Phys.* **1998**, *108*, 4439.

[23] D. Andrae, U. Häussermann, M. Dolg, H. Stoll, H. Preuss, *Theor. Chim. Acta.* **1990**, *77*, 123.

[24] A. W. Ehlers, M. Böhme, S. Dapprich, A. Gobbi, A. Höllwarth, V. Jonas, K. F. Köhler, R. Stegmann, A. Veldkamp, G. Frenking, *Chem. Phys. Lett.* **1993**, *208*, 111.

[25] a) W. J. Hehre, R. Ditchfield, J. A. Pople, *J. Chem. Phys.* **1972**, *56*, 2257; b) P. C. Hariharan, J. A. Pople, *Theor. Chim. Acta.* **1973**, *28*, 213; c) M. M. Francl, W. J. Pietro, W. J. Hehre, J. S. Binkley, M. S. Gordon, D. J. Defrees, J. A. Pople, *J. Chem. Phys.* **1982**, *77*, 3654.

Received: September 14, 2012